International Journal of Fluid Mechanics & Thermal Sciences
2024; 10(2): 31-44
http://www.sciencepublishinggroup.com/j/ijfmts
doi: 10.11648/j.ijfmts.20241002.12
ISSN: 2469-8105 (Print); ISSN: 2469-8113 (Online)

Hydromagnetic Nanofluid Flow Through Stretching Convergent-divergent Conduit with Heat and Mass Transfer

Paul Wachira Githaiga*, Mathew Ngugi Kinyanjui, Roy Phineas Kiogora

Department of Pure and Applied Mathematics, Jomo Kenyatta University of Agriculture and Technology, Nairobi, Kenya

Email address:

wachipaul@gmail.com (Paul Wachira Githaiga), mathewkiny@jkuat.ac.ke (Mathew Ngugi Kinyanjui),
Prkiogora@fsc.jkuat.ac.ke (Phineas Roy Kiogora)
*Corresponding author

To cite this article:

Paul Wachira Githaiga, Mathew Ngugi Kinyanjui, Roy Phineas Kiogora. (2024). Hydromagnetic Nanofluid Flow Through Stretching Convergent-divergent Conduit with Heat and Mass Transfer. *International Journal of Fluid Mechanics & Thermal Sciences, 10*(2), 31-44. https://doi.org/10.11648/j.ijfmts.20241002.12

Received: 29 September 2024; **Accepted:** 22 October 2024; **Published:** 18 November 2024

Abstract: This present study investigates hydromagnetic non-Newtonian nanofluid flow past linearly stretching convergent-divergent conduit with variable magnetic field and variable thermal conductivity with skin friction, heat and mass transfer using spectral relaxation numerical technique. The nanofluid considered in this current study is electrically conducting which is subjected to constant pressure gradient and magnetic field considered to be variable applied at an angle. The two walls which are non-parallel are not intersecting so as to allow nanofluid to flow, the angle in between the non-parallel walls is θ. The equations governing the nanofluid flow are continuity, energy, magnetic induction and conservation of momentum equations. After modelling, the specific equations governing the nano-fluid flow are partial differential equations which are highly nonlinear, the specific equations are first transformed through similarity transformation into a systems of ordinary differential equations. The boundary value problem formed is solved numerically using spectral relaxation numerical technique. The results of effects of varying various dimensionless parameters of the model are represented graphically and results discussed at each stage. The knowledge of nanofluids can be used in nuclear power production where it acts as a coolant. In Africa, South Africa is the only country producing nuclear power for commercial use, different governments on the continent are exploring nuclear energy as a climate-friendly for power production to enhance industrialization even in rural areas. In nuclear power production, water is used as a coolant. Using nanofluid instead of water it could increase the thermophyical properties which increases the rate of cooling. The usage of nanofluids as a coolant could also be used in emergency cooling systems, where they could cool down overheat machines quickly leading to an efficient and improved power plant safety.

Keywords: Hydromagnetic, Spectral Relaxation Method, Skin Friction, Heat and Mass Transfer

1. Introduction

Nanofluids are dilute suspension of nanosized particles suspended in a base fluid with the particles which are less than one hundred nanometre. From studies which have been carried out, nanofluids have exhibited improved thermophysical properties enhancement such as thermal conductivity, thermal diffusivity, electrical conductivity, viscosity and heat transfer. Heat transfer through convection currents in nanofluids is high and efficient as compared water as base fluids. Concerning this, nanotechnology is one of the growing and active research areas by researchers and scientists recently due to its' vast applications in solving real-world problems.

In recent years nanotechnology has been applied in several industrial applications to enhance the surroundings i.e. existing pollution cleaning, improving manufacturing methods to enhance the reduction of pollution, making alternative energy sources more cost-effective and cooling of atomic engines. The Republic of South Africa stands as the sole African nation engaging in the commercial production of nuclear power. Meanwhile, other governments across the continent are actively exploring nuclear energy as a sustainable and environmentally friendly substitute for traditional fossil

fuels. As of 2018, the International Atomic Energy Agency (IAEA) reported that at least ten additional African countries were contemplating the integration of nuclear power. The IAEA, an organization dedicated to promoting the peaceful use of nuclear energy, highlights the potential of nuclear technology not only in generating electricity but also in addressing critical development challenges, particularly in a continent with a population of approximately 1.2 billion people. In recent years, an increasing number of African nations have expressed keen interest in establishing nuclear power programs to alleviate existing power deficiencies. It is estimated that as of 2019, around 600 million people on the continent lack access to electricity, while approximately 900 million people do not have access to clean cooking fuel. Consequently, nuclear energy is being recognized as a crucial component of Africa's energy portfolio, aligning with the United Nations' Sustainable Development Goals and the African Union's vision for 2030 and Agenda 2063, both of which emphasize the importance of ensuring affordable, reliable, and sustainable modern energy access and food security for the African population.

Makinde O, D studied critical analysis of the influence of magnetic Reynolds number on MHD Jeffery - Hamel flow [1]. After the modelling non-dimensional parameters were obtained. The observation was when Reynolds number increases, it led to decreament in fluid velocity in the free stream region of the conduit and on increasing the Hartman you are controlling the effect of backflow reduction. Variable thermal conductivity and variable magnetic field was not taken into account. The rate of skin friction, heat and mass transfer was not taken into consideration. This is a gap and needs to be addressed. Furthermore, the numerical technique employed to solve the equations arising from the study needs to be re-looked and solve the equations with a current efficient method for solving ordinary differential equations.

Moffat, W, did an investigation on the effect of MHD on Jeffery-Hamel flow [2]. They found analytically that the speed discontinuity of the flowing fluid was gradually increasing on increasing the Reynolds number. The method used was analytical method and numerical methods require to be included to obtain the desired results. In our model, we have used spectral relaxation method to solve the arising model of systems of ordinary differential equations. The rate of skin friction, heat and mass transfer was not taken into consideration. This is an area which needs consideration due to the effects of velocity on rate of friction.

Voropayev, S, I found similar solutions on investigating two-dimensional steady-state incompressible viscous flow problem of non-Newtonian fluid inside the convergent-divergent cone with and without sink source [3]. They found that for viscoelastic fluids, they is a delay of flow separation in a diverging channel provided the inclined magnetic field which is applied either perpendicular or inclined is sufficiently strong. They used separation of variables technique to solve the arising models of equation. The observation was that increase in α leads to decrease in magnetic Reynolds number and the converse is true. This shows that both the channel angle and Reynolds number have an inverse relationship. It was also observed that on increasing Reynolds number, it led to decreasing velocity field and on increasing Hartman number it led to decreasing the back flow reduction. In this research the effects of stretching was not taken into account, the rate of skin friction, heat and mass transfer was not taken into consideration, unsteady state of the fluid flow and variable thermal conductivity needs to be addressed.

Ojiambo, V and Kimathi, M and Kinyanjui, M, studied two-phase Jeffery Hamel flow in a geothermal pipe concentrated with silica particles and thermophoresis [4]. Similarity transformation was applied to transform the arising non-linear partial differential equations to non-linear ordinary differential equations. Using an inbuilt bvp4c matlab solver was employed to solve the arising non-linear ordinary differential equations. The observation was that increasing the unsteadiness parameter; λ had effect on flow variables. On increasing the unsteadiness parameter lead to decrease of temperature and concentration profiles in gaseous and also in liquid phase. The rate of skin friction, heat and mass transfer was not taken into consideration. The effect of magnetic field, variable thermal conductivity, nanofluid and stretching walls is a gap which needs to be addressed.

Githaiga, Paul Wachira and Kinyanjui, Mathew Ngugi and Giterere, Kangethe and Kogora, Phineous Roy, investigated magnetohydrodynamics fluid flow in convergent-divergent conduit in the presence of constant pressure gradient and uniform magnetic field applied at an angle to the fluid flow direction and taking into account the effects of Joule heating parameter [5]. The resulting partial differential equations governing the model were first transformed to ordinary differential equations using the similarity transformations. The results obtained were represented in a graphical manner. The observation was that on increasing joule heating parameter led to increment in velocity and and temperature profiles in the fluid flow region. They also observed that when you increase the Hartman number, there is reduction of velocity in the flow region. In view of the above research, there is a gap of nano-fluid, variable thermal conductivity, variable magnetic applied at an angle, the effect of stretching of the non-parallel walls and skin friction, heat and mass transfer which needs to be addressed.

Sheikholeslami, Mohsen and Rokni, Houman B, investigated simulation of nanofluid heat transfer in presence of constant magnetic field. In this study they considered constant magnetic field [6]. The numerical method to solve the arising system of equations is pertubation method. They observed that temperature gradient augments with augment of solid particle concentration and buoyancy forces, while it decreases with augment of magnetic field. In this study, Joule heating was not taken into consideration, the viscosity of the nanofluid was assumed to be constant but non-Newtonian fluids are industry oriented and magnetic field should be considered to be variable and applied at an angle. The rate of skin friction, heat and mass transfer was not taken into consideration. The above are some of the gaps which needs to be addressed.

Kaigalula, Victor and Mutua, Samuel, examined numerical study for soret and dufour effects considering unsteady Newtonian MHD fluid flow with mass and heat transfer in a collapsible elastic tube using Spectral Collocation numerical technique [7]. The governing equations of the model were partial differential equations, they used similarity transformation to transform PDEs to ODEs. The ordinary differential equations formed were linear and were solved using the collocation method and were implemented in MATLAB using inbult bvp4c. The fluid considered here was Newtonian fluid. The results were represented in graphs and in tabular form. They observed that increasing Hartman number reduces the velocity. With regard of the above, non-Newtonian fluid, nanofluid, variable thermal conductivity and variable magnetic field applied at angle have not been addressed. This present study will address gaps.

Githaiga, P. W., Kinyanjui, M. N., Kiogora, R. P, investigated hydromagnetic non-Newtonian nanofluid flow past linearly stretching convergent-divergent conduit with chemical reaction [8]. They transformed partial differential equations to ordinary differential equations through similarity transformation. They observed that increasing the Hartman parameter leads to decrease of nano-fluid velocity in the flow region, on increasing chemical reaction parameter leads to reduction in concentration profiles, It is observed that increasing solutal Grashof parameter leads to velocity to increase in the flow region and increasing Schmid number leads to a decrease in concentration profiles. The researchers did not consider effects of heating and magnetic field which has significant effect of thermophysical properties of nanofluids.

Renewable energy production is climatic friendly rather than fossils fuels not only in Africa but worldwide, Africa has high potential production of green energy which remains untapped. Nanofluids act as coolant in nuclear power production. South Africa is currently the sole African nation engaged in commercial nuclear power production, while other governments across the continent are considering nuclear energy as a more environmentally friendly substitute for fossil fuels. In a pressurized water reactor (PWR) nuclear power plant system, the critical heat flux (CHF) process is a key factor in steam generation, as the presence of vapor bubbles on the fuel rod surface hinders heat conduction compared to liquid water. By employing nanofluids instead of water, the fuel rods can be coated with nanoparticles like alumina, which actively disperse newly formed bubbles, thereby preventing the buildup of a vapor layer around the rod and significantly enhancing the critical heat flux. The application of nanofluids as a coolant could also be beneficial in emergency cooling systems, as they have the potential to swiftly reduce overheated surfaces, consequently leading to improved power plant safety.

The present research considers hydromagnetic non-Newtonian nanofluid through convergent-divergent conduit with variable thermal conductivity and variable magnetic field. This research has taken into considerations the above stated gaps so as to enhance production of green energy in African continent and has been addressed.

2. Mathematical Modeling

2.1. Geometry of the Study

The geometry of the research problem is as below:

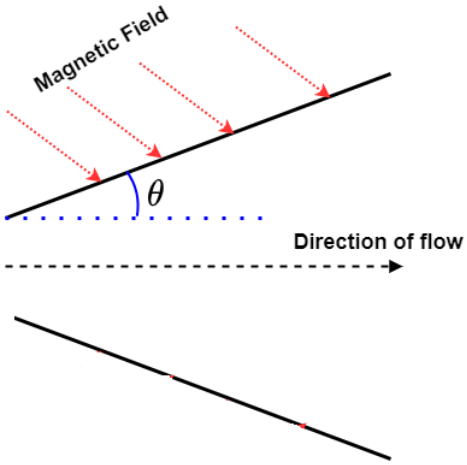

Figure 1. *Configuration of the problem.*

2.2. Assumptions

The nanofluid particles move in layers, thus we are considering laminar flow. The nanofluid flow is assumed to flow in radial direction, $u_r \gg u_\theta$ and the flow along along u_z and u_θ is negligible. The fluid flow is unsteady, density of the nanofluid is assumed to be incompressible i.e density assumed to be constant but variable in bouyancy term. Thermal conductivity is a variable and Viscosity is a non-linear function of the tangential direction θ and temperature T.

2.3. Governing Equations

The equations governing this present nanof;uid flow study are Continuity, Energy, Magnetic induction and Concentration which are given respectively as:

Continuity equation:

$$\frac{1}{r}\frac{\partial(ru_r)}{\partial r} + \frac{1}{r}\frac{\partial(u_\theta)}{\partial \theta} = 0 \tag{1}$$

Since $u_r \gg u_\theta$, equation (1) reduces to:

$$\frac{1}{r}\frac{\partial(ru_r)}{\partial r} = 0 \tag{2}$$

Equation (2) represents the equation of continuity in cylindrical coordinates for a two-dimensional unsteady, laminar flow of an incompressible fluid whose motion is purely in radial direction i.e. the flow is axisymmetric.

The equation of continuity must be satisfied for any possible fluid flow.

Equation of conservation of momentum:

$$\rho_{nf}\frac{\partial u_r}{\partial t} = -\frac{\partial P}{\partial r} - u_r\rho_{nf}\frac{\partial u_r}{\partial r} + \mu_{nf}[\frac{1}{r}\frac{\partial u_r}{\partial r} + \frac{\partial^2 u_r}{\partial r^2} - \frac{u_r}{r^2} + \frac{1}{r^2}\frac{\partial^2 u_r}{\partial \theta^2}]+$$
$$\frac{1}{r^2}\frac{\partial \mu_{nf}}{\partial \theta}\frac{\partial u_r}{\partial \theta} + g_r\rho_{nf}[\beta_T(T-T_\infty)+\beta_C(C-C_\infty)]$$
$$-\rho_{nf}[\mu_e^2\sigma u_r(\mathbf{H}_\theta^* - \mathbf{H}_0 sin\alpha)(\mathbf{H}_\theta^* + \mathbf{H}_0 cos\alpha)] \tag{3}$$

Energy Equation:

$$\frac{\partial T}{\partial t} + u_r\frac{\partial T}{\partial r} = \frac{b\kappa_{nf}^*}{\rho_{nf}(C_p)_{nf}\triangle T}(\frac{\partial T}{\partial r})^2 + \frac{1}{\rho_{nf}(C_p)_{nf}r^2}\frac{b\kappa_{nf}^*}{\triangle T}(\frac{\partial T}{\partial \theta})^2$$
$$+\frac{\kappa_{nf}^*}{\rho_{nf}(C_p)_{nf}}[1+b\frac{T-T_\infty}{\triangle T}][\frac{\partial^2 T}{\partial^2 r} + \frac{1}{r}\frac{\partial T}{\partial r} + \frac{1}{r^2}\frac{\partial^2 T}{\partial^2 \theta}] + \frac{\mu_{nf}\phi}{\rho_{nf}(C_p)_{nf}}+$$
$$\frac{\sigma_{nf}[\mu_e u_r(\mathbf{H}_\theta^* - \mathbf{H}_0 sin\alpha)]^2}{\rho_{nf}(C_p)_{nf}} \tag{4}$$

$$\mu_{nf}\phi = 2\mu_{nf}[(\frac{\partial u_r}{\partial r})^2 + (\frac{u_r}{r})^2] + \mu_{nf}[(\frac{1}{r}\frac{\partial u_r}{\partial \theta})^2] \tag{5}$$

Concentration equation:

$$\frac{\partial C}{\partial t} + u_r\frac{\partial C}{\partial r} = D_f(\frac{1}{r}\frac{\partial C}{\partial r} + \frac{\partial^2 C}{\partial r^2} + \frac{1}{r^2}\frac{\partial^2 C}{\partial \theta^2}) - k_r C \tag{6}$$

Boundary conditions considered are as follows.
At the center line at $\theta = 0$:

$$u_r = u_\infty, T = T_\infty, C = C_\infty, H_\theta = 0 \tag{7}$$

on the walls of the plate at $\theta = \alpha$:

$$\frac{\partial u_r}{\partial \theta} = -\gamma u(\theta), T = T_w, C = C_w, H_\theta = H_\infty \tag{8}$$

3. Thermophysical Properties

Nanofluids enhance the rate of increase of heat transfer in nanofluids via convectional currents. Thermo-physical properties of the nano-fluids are important for determining the rate and behavior of heat transfer. For example, the thermal conductivity of the nanofluids depends on the volume fraction, base fluid material, particle material and the temperature. In this present study we have taken consideration of copper-water nanoparticles so that we increase the thermophysical properties of the water.

The following is the thermophysical properties of the base fluid which is pure water and copper (Cu) as the nano-particles as Mutuku-Njane, WN and Makinde, OD [9].

The following are the thermophysical expressions related to this present study.

Table 1. *Thermophysical properties of the base fluid (pure water) and Copper (Cu) as the nanoparticles.*

Thermophysical properties	$\rho(kg/m^3)$	$c_p(J/kgK)$	$\kappa(W/mK)$	$\beta \times 10^{-5}(K^{-1})$	$\sigma(S/m)$
Pure Water	997.1	4179	0.613	21	5.5×10^{-6}
Copper (Cu)	8933	385	401	1.67	59.6×10^{6}

The following are the thermophysical expressions related to this present study;

$$\frac{\sigma_{nf}}{\rho_{nf}} = \frac{\sigma_f}{\rho_f}\left[\frac{(1-\Psi)+\Psi\frac{\sigma_s}{\sigma_f}}{(1-\Psi)+\Psi\frac{\rho_s}{\rho_f}}\right] = \frac{\sigma_f}{\rho_f}A \tag{9}$$

$$\frac{\mu_{nf}}{(\rho C_p)_{nf}} = \frac{\mu_f}{(\rho C_p)_f}\left[\frac{(1-\Psi)^{-2.5}}{(1-\Psi)+\Psi\frac{(\rho C_p)_s}{(\rho C_p)_f}}\right] = \frac{\mu_f}{(\rho C_p)_f}B \tag{10}$$

$$\frac{\mu_{nf}}{\rho_{nf}} = \frac{\mu_f}{\rho_f}\left[\frac{(1-\Psi)^{-2.5}}{(1-\Psi)+\Psi\frac{\rho_s}{\rho_f}}\right] = \frac{\mu_f}{\rho_f}C \tag{11}$$

$$\frac{k_{nf}}{(\rho C_p)_{nf}} = \frac{k_f}{(\rho C_p)_f}\left[\frac{\frac{(k_s+2k_f)-2\Psi(k_f-k_s)}{k_s+2k_f+\Psi(k_f-k_s)}}{(1-\Psi)+\Psi\frac{(\rho C_p)_s}{(\rho C_p)_f}}\right] = \frac{k_f}{(\rho C_p)_f}D \tag{12}$$

$$(\rho C_p)_{nf} = (\rho C_p)_f\left[(1-\Psi)+\Psi\frac{(\rho C_p)_s}{(\rho C_p)_f}\right] = (\rho C_p)_f E \tag{13}$$

$$\rho_{nf} = \rho_f\left[(1-\Psi)+\Psi\frac{\rho_s}{\rho_f}\right] = \rho_f M \tag{14}$$

$$\sigma_{nf} = \sigma_f\left[(1-\Psi)\sigma_f+\Psi\frac{\sigma_s}{\sigma_f}\right] = \sigma_f N \tag{15}$$

$$\frac{k*}{(C_p)_{nf}} = \frac{k_f}{(C_p)_f}\left[\frac{\frac{(k_s+2k_f)-2\Psi(k_f-k_s)}{k_s+2k_f+\Psi(k_f-k_s)}}{(1-\Psi)+\Psi\frac{(C_p)_s}{(C_p)_f}}\right] = \frac{k_f}{(C_p)_f}S \tag{16}$$

$$(C_p)_{nf} = (C_p)_f\left[(1-\Psi)+\Psi\frac{(C_p)_s}{(C_p)_f}\right] = (C_p)_f L \tag{17}$$

4. Similarity Transformation

From Nagler, J, and Githaiga, P. W., Kinyanjui, M. N., Kiogora, R. P, among other researchers, the following similarity transformations are used in order to transform the specific equations of the fluid flow model from partial differential equations to ordinary differential equations [10].

$$u_r(r,\theta,t) = -\frac{Q}{r}\frac{1}{\delta^{m+1}}f(\theta) \tag{18}$$

$$\frac{\phi(\theta)}{\delta^{m+1}} = \frac{C-C_\infty}{C_w-C_\infty} \tag{19}$$

$$\frac{\omega(\theta)}{\delta^{m+1}} = \frac{T-T_w}{T_\infty-T_w} \tag{20}$$

$$\mu = \mu_0\theta^{c(n-1)} \tag{21}$$

$$\mathbf{H}_\theta(r,\theta,t) = -\frac{Q}{r}\frac{1}{\delta^{m+1}}\varphi(\theta) \tag{22}$$

$$\mathbf{H}_r(r,\theta,t) = -\frac{Q}{r}\frac{1}{\delta^{m+1}}\gamma(\theta) \tag{23}$$

Where $\omega(\theta)$ is dimensionless temperature, $f(\theta)$ is dimensionless velocity, $\phi(\theta)$ is the dimensionless concentration, T_∞ is the temperature at the center of the conduit,T_w is the temperature at the wall, is the concentration at the wall, δ is the time-dependent length scale and m are arbitrary constant which is wedge angle related.

On transforming equations (3), (4) and (6) the equations reduces to:

$$\rho_{nf}\frac{\partial u_r}{\partial t} = -u_r\rho_{nf}\frac{\partial u_r}{\partial r}+\mu_{nf}[\frac{1}{r}\frac{\partial u_r}{\partial r}+\frac{\partial^2 u_r}{\partial r^2}-\frac{u_r}{r^2}+\frac{1}{r^2}\frac{\partial^2 u_r}{\partial\theta^2}]+\frac{1}{r^2}\frac{\partial\mu_{nf}}{\partial\theta}\frac{\partial u_r}{\partial\theta}$$

$$+g_r\rho_{nf}[\beta_T(T-T_\infty)+\beta_C(C-C_\infty)]-\rho_{nf}[\mu_e^2\sigma u_r(\mathbf{H}_\theta^*-\mathbf{H}_0 sin\alpha)(\mathbf{H}_\theta^*+\mathbf{H}_0 cos\alpha)] \tag{24}$$

$$-(T_\infty-T_w)\frac{m+1}{\delta^{m+2}}\frac{d\delta}{dt}\omega = \frac{1}{\rho_{nf}(C_p)_{nf}r^2}\frac{b\kappa_{nf}^*}{(T_\infty-T_w)}((T_\infty-T_w)\frac{\omega^{'}}{\delta^{m+1}})^2+\frac{\kappa_{nf}^*}{\rho_{nf}(C_p)_{nf}}b\frac{T-T_\infty}{T_\infty-T_w}\frac{1}{r^2}(T_\infty-T_w)\frac{\omega^{''}}{\delta^{m+1}}+$$

$$\frac{\kappa_{nf}^*}{\rho_{nf}(C_p)_{nf}}\frac{1}{r^2}(T_\infty-T_w)\frac{\omega^{''}}{\delta^{m+1}}+\frac{\mu_0\theta^{c(n-1)}}{\rho_{nf}(C_p)_{nf}}[2(\frac{Q}{r^2}\frac{1}{\delta^{m+1}}f)^2+2\frac{1}{r^2}(-\frac{Q}{r}\frac{1}{\delta^{m+1}}f)^2+$$

$$\frac{1}{r^2}(-\frac{Q}{r}\frac{1}{\delta^{m+1}}f^{'})^2]+\frac{\sigma_{nf}\mu_e^2(\mathbf{H}_\theta^*-\mathbf{H}_0 sin\alpha)^2}{\rho_{nf}(C_p)_{nf}}\frac{Q^2}{r^2}\frac{1}{\delta^{2m+2}}f^2 \tag{25}$$

$$-(C_W - C_\infty)\frac{m+1}{\delta^{m+2}}\frac{d\delta}{dt}\phi = D_f\frac{(C_w - C_\infty)}{r^2}\frac{\phi^{''}(\theta)}{\delta^{m+1}} - k_r C \tag{26}$$

On simplifying and introducing the dimensionless parameters arising from the study as listed below:

$$\lambda = \frac{\rho_f \delta^m}{\mu_0 r^{m-1}}\frac{d\delta}{dt}, Re = \frac{Q\rho_f}{\mu_0}, Gr_T = \frac{g_r\rho_f}{\mu_o}r^3\beta_T(T_w - T_\infty),$$

$$Gr_C = \frac{g_r\rho_f}{Q\mu_o}r^3\beta_C(C_w - C_\infty), Sc = \frac{\mu_0}{D_f\rho_f} \tag{27}$$

Where Re is Reynolds number, Gr_T is Thermal Grashof number, Gr_c is solutal Grashof number, Sc is Schmidt number, λ is Unsteadiness parameter and.

On substituting equations (27) and equations (9) to (17) into equations (24) to (26), the equations reduces to:

$$(m+1)r^{m+1}\lambda Mf = MRef^2 - c(n-1)\delta^{m+1}f^{''} - c(n-1)$$

$$\theta^{c(n-1)-1}\delta^{m+1}f^{'} + M\frac{Gr_T}{Q}\omega\delta^{m+1} + M\frac{Gr_C}{Q}\phi\delta^{m+1} + MNHa^2\delta^{m+1}f \tag{28}$$

$$-M(m+1)\frac{r^{m+1}}{\delta^{m+1}}\lambda\omega = \frac{S}{Pr}[b\omega\delta^{m+1} + \frac{b\omega}{\delta^{m+1}} - b + \omega^{''}] + \frac{Ec}{L}\theta^{c(n-1)}\delta^{m+1}[4f^2 + f^{'2}] + \frac{N}{L}J\delta^{m+1}f^2 \tag{29}$$

$$-M(m+1)\lambda r^{m+1}\phi = \frac{M}{Sc}\phi^{''}\delta^{m+1} - Mk_r\delta^{2m+2} \tag{30}$$

The transformed Boundary conditions are as follows,

At the centerline $\theta = 0$ is

$$f(0) = -\frac{ru_\infty\delta^{m+1}}{Q}, f^{'}(0) = 0, \omega^{'}(0) = 0, \phi(0) = 0, \phi^{'}(0) = 0, \tag{31}$$

At the wall, $\pm\alpha$ is

$$f(\pm\alpha) = 0, f^{'}(\pm\alpha) = -\gamma f(\theta), \omega(\pm\alpha) = 0, \phi(\pm\alpha) = \delta^{m+1}, \varphi(\pm\alpha) = -\frac{r}{Q}\delta^{m+1}H_\infty \tag{32}$$

5. Numerical Solution Procedure

5.1. Spectral Relaxation Model

This method is based on developing the system of non-linear ordinary differential equations using Relaxation technique and applying spectral collocation in the discretization of linearized system, as iluustrated by [11].

In the Relaxation method framework, the systems of non-linear ODEs equations (28), (29) and (30) are written as:

5.2. Relaxation Scheme on Governing Equations

5.2.1. Momentum Equation

$$L_1[f, \omega, \phi] + N_1[f, \omega, \phi] = 0 \tag{33}$$

5.2.2. Energy Equation

$$L_2[f, \omega, \phi] + N_2[f, \omega, \phi] = 0 \tag{34}$$

5.2.3. Concentration Equation

$$L_3[f, \omega, \phi] + N_3[f, \omega, \phi] = 0 \tag{35}$$

The relaxation scheme of the equations (33), (34) and (35) respectively is given by:

$$L_1[f_{r+1}, \omega_r, \phi_r] + N_1[f_r, \omega_r, \phi_r] = 0 \tag{36}$$

$$L_2\left[f_{r+1},\omega_{r+1},\phi_r\right]+N_2\left[f_{r+1},\omega_r,\phi_r\right]=0 \tag{37}$$

$$L_4\left[f_{r+1},\omega_{r+1},\phi_{r+1}\right]+N_4\left[f_{r+1},\omega_{r+1},\phi_r\right]=0 \tag{38}$$

Where $r+1$ and r in equations (36), (37) and (38) denotes current and previous iteration levels respectively.
Rearranging equation (28), momentum along r direction reduces to:

$$(m+1)r^{m+1}\lambda Mf-MRef^2+c(n-1)\delta^{m+1}f^{''}+c(n-1)$$

$$\theta^{c(n-1)-1}\delta^{m+1}f^{'}-M\frac{Gr_T}{Q}\omega\delta^{m+1}-M\frac{Gr_C}{Q}\phi\delta^{m+1}-MNHa^2\delta^{m+1}f=0 \tag{39}$$

Relaxation scheme for the equation (39) is:

$$c(n-1)\delta^{m+1}f_{r+1}^{''}+c(n-1)\theta^{c(n-1)-1}\delta^{m+1}f_{r+1}^{'}+\left[(m+1)r^{m+1}\lambda M-MNHa^2\delta^{m+1}\right]f_{r+1}=MRef_r^2+$$

$$M\frac{Gr_C}{Q}\phi_r\delta^{m+1}+M\frac{Gr_T}{Q}\omega_r\delta^{m+1} \tag{40}$$

Considering energy equation, equation (29) and re-arranging we have:

$$-M(m+1)\frac{r^{m+1}}{\delta^{m+1}}\lambda\omega-\frac{S}{Pr}[b\omega\delta^{m+1}+\frac{b\omega}{\delta^{m+1}}-b+\omega^{''}]-\frac{Ec}{L}\theta^{c(n-1)}\delta^{m+1}[4f^2+f^{'2}]-\frac{N}{L}J\delta^{m+1}f^2=0 \tag{41}$$

Relaxation scheme for equation (41) (Energy Equation)is:

$$\frac{S}{Pr}\omega_{r+1}^{''}+\left[\frac{Sb\delta^{m+1}}{Pr}+\frac{Sb}{Pr\delta^{m+1}}+M(m+1)\frac{r^{m+1}}{\delta^{m+1}}\lambda\right]\omega_{r+1}=\frac{Sb}{Pr}$$

$$-\frac{Ec}{L}\theta^{c(n-1)}\delta^{m+1}[4f_{r+1}^2+f_{r+1}^{'2}]-\frac{N}{L}J\delta^{m+1}f_{r+1}^2 \tag{42}$$

Considering concentration equation, equation (30) and re-arranging we have:

$$-M(m+1)\lambda r^{m+1}\phi-\frac{M}{Sc}\phi^{''}\delta^{m+1}+Mk_r\delta^{2m+2}=0 \tag{43}$$

Relaxation scheme for equation (43) (Concentration equation)is:

$$\frac{M}{Sc}\delta^{m+1}\phi_{r+1}^{''}+M(m+1)\lambda r^{m+1}\phi_{r+1}=Mk_r\delta^{2(m+1)} \tag{44}$$

6. Spectral Collocation

The collocation method is a powerful numerical technique used to solve boundary value problems (BVP) by approximating the solution of ordinary differential equations (ODE) using polynomial functions. This method carefully selects a finite number of collocation points where the polynomial function accurately satisfies the ordinary differential equation (ODE). Various types of basis functions such as polynomials, trigonometric functions, etc., can be employed for the collocation method, and the selection of the basis function is tailored to the nature of the ODEs and the problem geometry. One notable advantage of the collocation method is its efficient use of solvers with low computational memory, making it a practical and implementable technique. This method is widely recognized as one of the most effective numerical approaches for solving BVP.

The approximation solution $f(\theta)$ for the momentum equation is assumed to be the Lagrange interpolating polynomial of the form:

$$f(\theta)=\sum_{j=0}^{N}L_j(\theta)\omega_j \tag{45}$$

Where

$$L_j(\theta)=\prod_{\substack{i=0\\ i\neq j}}^{N}\frac{\theta-\theta_i}{\theta_j-\theta_i} \tag{46}$$

is the Lagrange cardinal polynomial.

The grid points are the Chebyshev Gauss Lobatto points given by

$$\left\{cos\left(\frac{i\pi}{N}\right)\right\}_{i=0}^{N} \tag{47}$$

in the interval $[-1,1]$.

Appropriate linear transformation is applied to map the interval $[-1,1]$ to the computational domain at $[0,\alpha]$.

The first derivative of $\omega(\theta)$ is approximated by:

$$\omega^{'}(\theta) = \sum_{j=0}^{N} L_j^{'}(\theta)\omega_j \tag{48}$$

$\omega^{'}(\theta)$ is evaluated at the collocation points as

$$\omega^{'}(\theta_i) = \sum_{j=0}^{N} L_j^{'}(\theta_i)\omega_j = \sum_{j=0}^{N} D_{ij}\omega_j = D\omega \tag{49}$$

where D is the chebyshev differential matrix as defined by Mutuku-Njane, WN and Makinde, O. D and

$$\omega = [\omega(\theta_0), \omega(\theta_1), \omega(\theta_2), ..., \omega(\theta_N)]^T \tag{50}$$

Higher order discrete derivatives are approximated using matrix multiplication.

$$\omega^{'} = D\omega, \omega^{''} = D^2\omega, \omega^{'''} = D^3\omega \tag{51}$$

The derivatives for f and ϕ at the collocation points are approximated in similar manner.

Substituting the discrete derivatives in the linear relaxation scheme, equations (40), (42) and (44):

$$(c(n-1)\delta^{m+1}D^2 + c(n-1)\theta^{c(n-1)-1}\delta^{m+1}D + \left[(m+1)r^{m+1}\lambda M - MNHa^2\delta^{m+1}\right])F = R_1 \tag{52}$$

$$\left[\frac{S}{Pr}D^2 + \frac{Sb\delta^{m+1}}{Pr} + \frac{Sb}{Pr\delta^{m+1}} + M(m+1)\frac{r^{m+1}}{\delta^{m+1}}\lambda I\right]\omega = R_3 \tag{53}$$

$$\left[\frac{M}{Sc}\delta^{m+1}D^2 + M(m+1)\lambda r^{m+1}I\right]\Phi = R_4 \tag{54}$$

where R_1, R_3, and R_4 in equations (52), (53), and (54) are:

$$R_1 = MRef_r^2 + M\frac{Gr_C}{Q}\phi_r\delta^{m+1} + M\frac{Gr_T}{Q}\omega_r\delta^{m+1} \tag{55}$$

$$R_3 = \frac{Sb}{Pr} - \frac{Ec}{L}\theta^{c(n-1)}\delta^{m+1}[4f_{r+1}^2 + f_{r+1}^{'2}] - \frac{N}{L}J\delta^{m+1}f_{r+1}^2 \tag{56}$$

$$R_4 = Mk_r\delta^{2(m+1)} \tag{57}$$

Transforming the boundary conditions using transformations equations (18) to (21), we have:
At the pipe wall, $\theta = \pm\alpha$

$$f(\pm\alpha) = 0, f^{'}(\pm\alpha) = -\gamma f(\theta), \omega(\pm\alpha) = 0, \phi(\pm\alpha) = \delta^{m+1}, \varphi(\pm\alpha) = -\frac{r}{Q}\delta^{m+1}H_\infty \tag{58}$$

At $\theta = 0$, the interface is treated as a moving wall

$$f(0) = -\frac{u_\infty\delta^{m+1}}{Q}, f^{'}(0) = 0, \omega(0) = \delta^{m+1}, \omega^{'}(0) = 0, \phi(0) = 0, \phi^{'}(0) = 0, \varphi(0) = 0 \tag{59}$$

At the entry point, $(r = 0)$ the flow is not fully developed and we have

$$f(0) = -\frac{u_\infty\delta^{m+1}}{Q}, \omega(0) = \delta^{m+1}, \omega^{'}(0) = 0, \phi(0) = 0, \phi^{'}(0) = 0, \varphi(0) = 0 \tag{60}$$

At the exit point $(r = \infty)$, the gradients of all variables in the flow directions is equals to zero.

$$\frac{\partial f}{\partial r} = 0, \frac{\partial \omega}{\partial r} = 0, \frac{\partial \varphi}{\partial r} = 0, \frac{\partial \phi}{\partial r} = 0 \tag{61}$$

7. Results and Discussion

The numerical solutions of the models' velocity,temperature, induction and concentration profiles while varying various non-dimensional parameters are represented as graphs below. The effect of each dimensionless parameter has been discussed at each stage.

7.1. Effects of Varying Unsteadiness Parameter on Temperature Profiles

Unsteadiness parameter caters for the unsteady state of the study being undertaken. From the graph, it is observed increasing the unsteadiness parameter leads to velocity to reduce in the flow region. As the fluid flows from converging section to diverging section, the surface area reduces and it flows down the flow region hence reducing the velocity. This will in turn lead to improved heat transfer hence leading to efficient cooling.

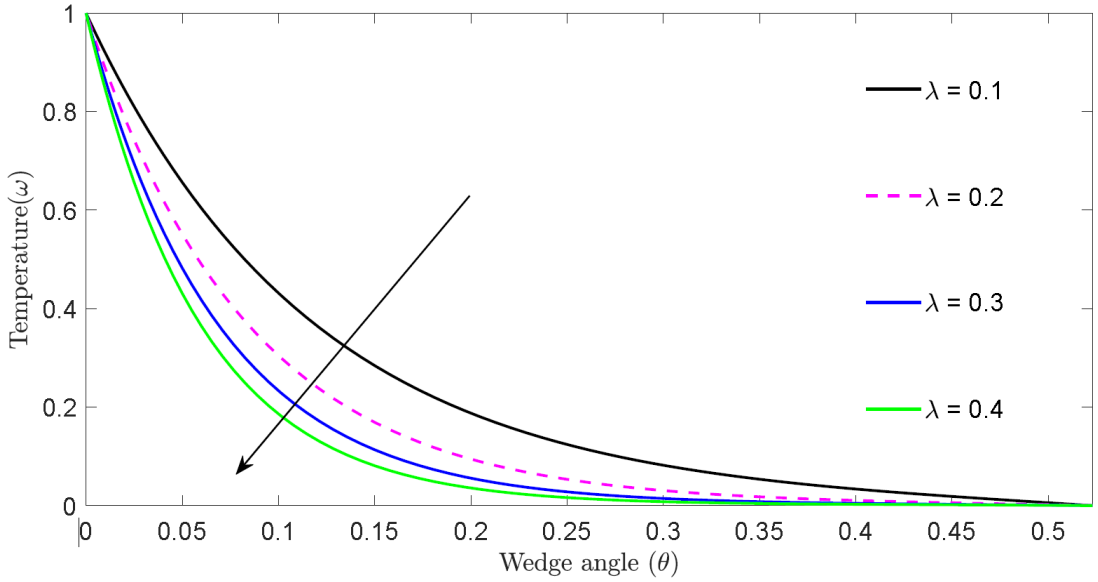

Figure 2. *Graph of dimensionless temperature profiles for varying unsteadiness parameter*

7.2. Effects of Varying Prandtl Number on Temperature Profiles

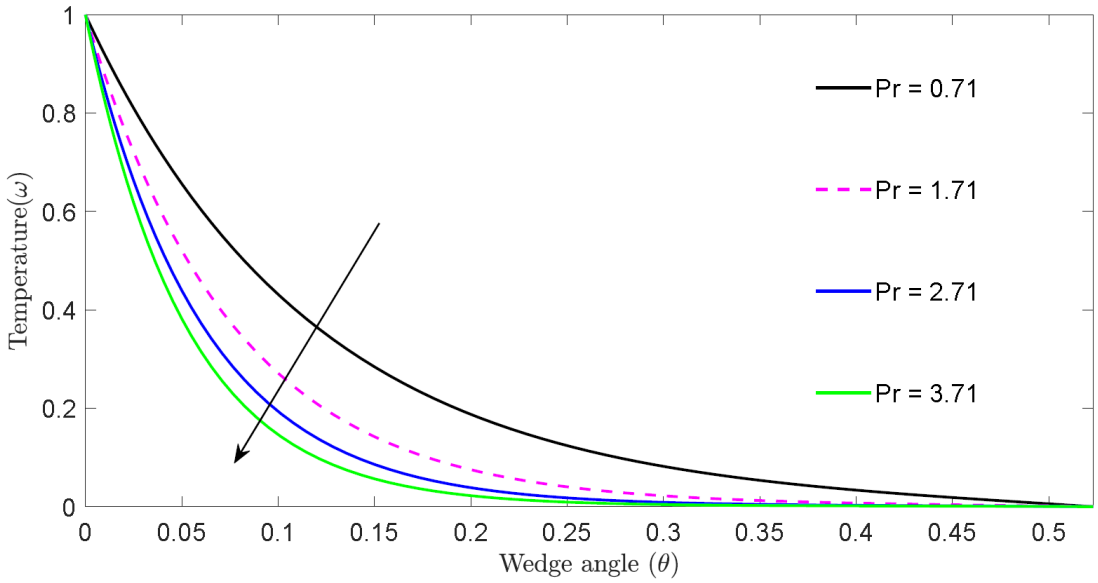

Figure 3. *Graph of dimensionless temperature profiles for different Prandtl number*

Prandtl number is the ratio between momentum diffusivity(viscosity) and heat diffusivity(thermal). From temperature profile graph above, it is observed increasing Prandtl number reduces the nano-fluid velocity in the flow region. Increasing Prandtl number enhances viscosity and it becomes predominant more than thermal diffusivity hence leading to reduced velocity in the flow region.

8. Skin Friction Coefficient, Mass Transfer and Heat Transfer Rates

For this study, the physical parameters of engineering interest are Skin friction coefficient, the local Nusselt Number and the local Sherwood number.

Skin friction is the friction between nano-fluid particles in motion and the wall surface. The physical significance of skin friction coefficient is that it measures the energy loss as a result of friction between a surface and the nano-fluid flowing over it.

The rate of heat transfer is defined as heat transfer rate in the nano-fluid particles.

Mass transfer can be defined as movement of species in a mixture from a high concentrated region to a low concentrated region.

Nusselt number indicates the magnitude of convectional heat transfer across a fluid boundary.

Sherwood number indicates the ratio of convective mass transfer to diffusive mass transport. This number measures the enhancement of mass transfer due to convection. Movement of nano-fluid particles can increase the rate of mass transfer significantly.

In this study Skin Friction, Nusselt number and Sherwood number are as defined by Mutuku-Njane, WN and Makinde, OD respectively [9].

$$\frac{1}{2}S_f\sqrt{2-\Omega} = Re^{\frac{1}{2}}f^{'}(0) \tag{62}$$

$$Nu\sqrt{2-\Omega} = -Re^{-\frac{1}{2}}\omega^{'}(0) \tag{63}$$

$$Sh\sqrt{2-\Omega} = -Re^{-\frac{1}{2}}\phi^{'}(0) \tag{64}$$

Effects of Variation of Parameters on Skin Friction

Table 2. *Effects of variation of parameters on skin friction.*

Re	Gr_T	Gr_C	Ha	Ec	λ	$Cf(SkinFriction)$
4.2	10	10	2	1.3	0.1	2.74093
6.2	10	10	2	1.3	0.1	2.91307
8.2	10	10	2	1.3	0.1	3.00872
10.2	10	10	2	1.3	0.1	3.08527
4.2	10	10	2	1.3	0.1	2.74093
4.2	20	10	2	1.3	0.1	2.29484
4.2	30	10	2	1.3	0.1	1.29141
4.2	40	10	2	1.3	0.1	2.28431
4.2	10	10	2	1.3	0.1	2.74093
4.2	10	20	2	1.3	0.1	2.62445
4.2	10	30	2	1.3	0.1	2.78458
4.2	10	40	2	1.3	0.1	3.00421
4.2	10	10	2	1.3	0.1	2.74093
4.2	10	10	3	1.3	0.1	2.72045
4.2	10	10	4	1.3	0.1	2.71333
4.2	10	10	5	1.3	0.1	2.64533
4.2	10	10	2	1.3	0.1	2.74093
4.2	10	10	2	2.3	0.1	2.75594
4.2	10	10	2	3.3	0.1	2.78994
4.2	10	10	2	4.3	0.1	2.83357
4.2	10	10	2	1.3	0.1	2.74093
4.2	10	10	5	1.3	0.2	2.74273
4.2	10	10	2	1.3	0.3	2.74194
4.2	10	10	2	1.3	0.4	2.75410

From the above table, the following observations are noted:

1. It is observed that on increasing Reynolds number it leads to increase in skin friction. The relationship is as a result of relationship between wall shear stress and the velocity gradient. As Reynolds number increases, the velocity of the nano-fluid increases which results to increased wall shear stress. Consequently this leads to increase in skin friction as Reynolds number is increased.
2. Increasing thermal Grashof number leads to increased skin friction coefficient. Increasing thermal Grashof number leads to increased velocity. The increased velocity of the nano-fluid flow leads to increment of skin friction coefficient.
3. Inreasing solutal Grashof number leads to increase in Skin friction coefficient. This is as a result, velocity boundary formed does not extend into the free stream region under high values of thermal Grashof number.

This in turn leads to increased velocity which in turn leads to increased skin friction coefficient.

4. It is observed that increasing Hartman leads to reduction of skin friction. On increasing the Hartman number, it leads to reduction of velocity as a result of induced Lorentz force. The Lorentz tends to oppose the velocity of the nano-fluid which in turn leads to reduced velocity and consequently reduction in skin friction.
5. Increasing the unsteadiness parameter has no or little significance on skin friction.
6. Increasing Eckert number leads to increased skin friction. The increased Eckert number leads to increased nanofluid velocity which leads to higher wall stress. This consequently increases the rate of skin friction.

Effects of Variation of Parameters on Heat Transfer Rate

Table 3. *Effects of variation of parameters on Heat transfer rate.*

Re	Gr_T	Gr_C	Ha	Ec	λ	$Nu(Heattransfer)$
4.2	10	10	2	1.3	0.1	3.82199
6.2	10	10	2	1.3	0.1	4.04021
8.2	10	10	2	1.3	0.1	4.19629
10.2	10	10	2	1.3	0.1	4.19395
4.2	10	10	2	1.3	0.1	3.82199
4.2	20	10	2	1.3	0.1	3.82222
4.2	30	10	2	1.3	0.1	3.82222
4.2	30	10	2	1.3	0.1	3.82222
4.2	10	10	2	1.3	0.1	3.82199
4.2	10	20	2	1.3	0.1	3.92001
4.2	10	30	2	1.3	0.1	3.94982
4.2	10	40	2	1.3	0.1	3.94984
4.2	10	10	2	1.3	0.1	3.82199
4.2	10	10	3	1.3	0.1	3.83000
4.2	10	10	4	1.3	0.1	3.83034
4.2	10	10	5	1.3	0.1	3.84404
4.2	10	10	2	1.3	0.1	3.82199
4.2	10	10	2	2.3	0.1	4.29021
4.2	10	10	2	3.3	0.1	4.65747
4.2	10	10	2	4.3	0.1	4.65749
4.2	10	10	2	1.3	0.1	3.82199
4.2	10	10	2	1.3	0.2	3.82200
4.2	10	10	2	1.3	0.3	3.83240
4.2	10	10	2	1.3	0.4	3.94901

The following are the observations from the table above:

1. Increase in Reynolds number leads to decrease in Nusselt number. This is as a result of, inreasing Reynolds number causes the thermal boundarly layer to thicken which in turn leads to decreament in Nullset Number.
2. Increase in thermal Grashof number has little or no effect on Nullset number.
3. Inreasing thermal Grashof number leads to increase in Nusselt number. Increased in velocity leads to increase in temperature gradient which in turn leads to increament in Nulsset number. The temperature gradient increases as the thermal boundary layer thickness decreases. The boundary layer thickness reduces for high flow rates, thus enhancing the heat transfer rate.
4. Increasing Hartman number leads to increase in heat transfer rate. This increase in Hartman parameter means that magnetic force dominates and viscous forces reduces. The increased magnetic force leads to thermal boundary layer to increase since the thermal boundary layer formed extends into the free stream region which in turn leads to an increased fluid temperature and hence increased rate of heat transfer resulting to increased Nulsset number.
5. Increase in unsteadiness parameter leads to increase in heat transfer rate. As the nano-fluid moves in the flow region all the kinetic energy of the nanofluid in motion is being converted in to heat due to vibration and bombardment of the nanofluid particles leading to heat dissipation. This causes the nanofluid to gain more heat as time increases and thus consequently increase in heat transfer rate as the nano-fluid flows.
6. Increasing Eckert number leads to increase in the rate of heat transfer. Increasing the Eckert leads to thermal boundarly layer thickness to decrease. The decreasing of the thermal boundary layer enhances the rate of the heat

transfer. The enhanced heat transfer due to to addition of nanoparticles to the base fluid enhances the rate of cooling in the cooling tower hence minimising cooling tower problems.

Effects of Variation of Parameters on Mass Transfer Rate

Table 4. *Effects of variation of parameters on Mass transfer rate.*

Re	Gr_T	Gr_C	K_r	Ec	S_c	$Sh(Masstransfer)$
4.2	10	10	0.01	1.3	0.03	6.05363
6.2	10	10	0.01	1.3	0.03	7.05457
8.2	10	10	0.01	1.3	0.03	9.04590
4.2	10	10	0.01	1.3	0.03	6.05363
4.2	20	10	0.01	1.3	0.03	6.06864
4.2	30	10	0.01	1.3	0.03	8.04534
4.2	10	10	0.01	1.3	0.03	6.05363
4.2	10	20	0.01	1.3	0.03	8.4690
4.2	10	30	0.01	1.3	0.03	10.4891
4.2	10	10	0.01	1.3	0.03	6.05363
4.2	10	10	0.02	1.3	0.03	10.3901
4.2	10	10	0.03	1.3	0.03	16.1037
4.2	10	10	0.01	1.3	0.03	6.05363
4.2	10	10	0.01	2.3	0.03	6.05373
4.2	10	10	0.01	3.3	0.03	6.05401
4.2	10	10	0.01	1.3	0.03	6.05363
4.2	10	10	0.01	1.3	0.04	5.72601
4.2	10	10	0.01	1.3	0.05	3.48304

The following are the observations from the table above:

1. Increasing in Reynolds number leads to increased mass transfer rate. Increasing Reynolds number leads to enhanced mass diffusivity of the nanoparticles in the nanofluid. This in turn leads to increase in mass transfer rate as Reynolds number increases.
2. Increasing thermal Grashof number leads to increased mass transfer rate. Increasing thermal grashof number leads to reduction of the thickness of the concentration boundary layer which increases the rate of the species transportation within this layer. As a result of this, the rate of mass transfer is enhanced.
3. Increasing solutal grashof number leads to increased mass transfer rate. Increasing the mass grashof number leads to thinning of concentration boundary layers. As a result of this, there is there is higher rate of transportation of nanoparticles in the nanofluid within these boundary layers which account for high rate of mass transfers.
4. Increasing the rate of chemical reaction increases the rate of mass transfer. It increases the mass diffusivities of the nanoparticles which in turn implies more interactions of the species concentration with the momentum boundary layer thus increasing rate of mass transfer.
5. Increasing Eckert number increases the rate of mass transfer. This is as a result of, increasing Eckert number enhances the thickening of thermal boundary layer. Due to the thickening of thermal boundary layer, this enhances the species transportation consequently increasing the mass transfer rate.
6. Increasing Schimid numbers lowers the rate of mass transfer. There is decreased mass diffusivity i.e there is less interaction of the species concentration of the nanoparticles. This can lead to deposition of nanopraticles which can lead to scale formation and consequently can lead to inefficiency of the cooling.

Validation

To validate the presented results, the computed results are compared with the results of Githaiga, P. W., Kinyanjui, M. N., Kiogora, R. P, which proved to be in good agreement [8]. In absence of chemical reaction, variable thermal conductivity, induced magnetic field and stretching walls, the results are in agreement.

9. Conclusions

The following are conclusions made from graphs and tables:

1. Increasing Reynolds number leads to increase in skin friction, decrease in the rate of heat transfer and increased mass transfer rate.
2. Increasing the Hartman parameter leads to increase in skin friction coefficient, increase in heat transfer rate and had insignificant effects on mass transfer rate.
3. On increasing solutal Grashof parameter leads to increase in skin friction coefficient, increase in heat transfer rate and increased mass transfer rate.
4. It is observed that on increasing thermal Grashof number

leads to increased skin friction, it has no effect or little effect on heat transfer rate and increased mass transfer rate.

5. Increasing the unsteadiness parameter leads to reduction of concentration and reduction of magnetic induction. Increasing unsteadiness parameter has insignificant effect on skin friction and leads to increase in heat transfer rate.
6. On increasing chemical reaction parameter leads to increase in mass transfer rate.

Abbreviations

MHD	Magnetohydrodynamics
ODE	Ordinary Differential Equation
PDE	Partial Differential Equations
BVP	Boundary Value Probelem

Nomenclature

u_θ	Tangential velocity, rad ($rad\ s^{-1}$)
u_r	Radial velocity, meters (ms^{-1})
r	Radius of the tube, meters (m)
t	Time, seconds (s)
B_0	Applied magnetic field, Tesla (T)
κ	Variable thermal viscosity
T	Temperature, kelvin (K)
T_∞	Temperature at the center, kelvin (K)
T_w	Temperature at the wall, kelvin (K)
C	Concentration, mole per cubic meter mol/m^3
C_∞	Concentration at the center, mole per cubic meter mol/m^3
C_w	Concentration at the wall, mole per cubic meter mol/m^3
D_m	Concentration diffusion parameter, (m^2s^{-1})
k_r	Chemical reaction coefficient, (Ms^{-1})
Q	Discharge, (m^3s^{-1})
$f(\eta)$	Dimensionless velocity
P	Pressure, (Nm^{-2})
m	Arbitrary constant
I	Electric current, Ampere (A)
J	Electric current density, (Am^{-2})
$\overrightarrow{B}$	Magnetic vector
g	Gravitational force, (Nm^2kg^{-2})
q_h	Heat flux, (Wm^{-2})
q_m	Mass flux, ($kg\ m^{-2}s^{-1}$)
Re	Reynolds number
Ha	Hartmann number
Gr_T	Thermal Grashof number
Gr_c	Concentration Grashof number
Sc	Schmidt number
λ	Unsteadiness parameter
α	Thermal diffusion rate
β^c	Volumetric concentration expansion, ($kg\ m^{-3}$)
β^t	Volumetric thermal expansion, kelvin K^{-1}
ϕ	Chemical reaction parameter Ms^{-1}
δ	Time-dependent length scale, M
η	Dimensionless radius
λ	Unsteadiness parameter
μ	Fluid viscosity, $kg\ m^{-1}s^{-1}$
ρ_nf	Nano-Fluid density, kgm^{-3}
κ	Thermal conductivity, Wm^{-1}K^{-1}
τ	Shear stress, Nm^{-2}
σ	Electrical conductivity, $\Omega^{-1}m^{-1}$
τ_w	Skin shear stress, Nm^{-2}
θ	wedge angle, rad
$\omega(\theta)$	Dimensionless temperature
$\phi(\theta)$	Dimensionless concentration

Acknowledgments

Authors are grateful to the Pan African University Institute for Basic Sciences, Innovation and Technology(PAUSTI) for their support throughout the conduct of this present study.

Conflicts of Interest

We declare that we have no conflicts of interest.

References

[1] Makinde O, D, Investigatation of non-linear 2D Navier-Stokes equations modeling the flow field using a perturbation technique, International Journal of Engineering Sciences, 2008, 181(2), 966-972.

[2] Moffat, W, Effect of MHD on convergent divergent flow, Applied Mathematics and Computations, 2007, 225(2), 347-353.

[3] Voropayev, S I, Two−dimensional steady state incompressible viscous flow, Applied Mathematics and Computations, 2015, 20.

[4] Ojiambo, V and Kimathi, M and Kinyanjui, M, Int. J. of Adv. in Applied Math. and Mech, 5(4), 21–32, 2018.

[5] Githaiga, Paul Wachira and Kinyanjui, Mathew Ngugi and Giterere, Kangethe and Kogora, Phineous Roy, "Magneto Hydrodynamics Fluid Flow in Convergent-Divergent Conduit," International Journal of Engineering Science and Innovative Technology(IJESIT), 7(6), 1-10, 2018.

[6] Sheikholeslami, Mohsen and Rokni, Houman B, "Simulation of nanofluid heat transfer in presence of magnetic field: a review," International Journal of Heat and Mass Transfer, 115, 1203–1233, 2017, Elsevier.

[7] Kaigalula, Victor and Mutua, Samuel, Soret and Dufour Effects on MHD Fluid Flow Through a Collapssible Tube Using Spectral Based Collocation Method, Applied and Computational Mathematics, 13(1), 8–28, 2024.

[8] Githaiga, P. W., Kinyanjui, M. N., Kiogora, R. P, Hydromagnetic Non-Newtonian Nanofluid Flow Past Linealy Stretching Convergent-Divergent Conduit with Chemical Reaction, pplied and Computational Mathematics, 13(5), 130-139. https://doi.org/10.11648/j.acm.20241305.12

[9] Mutuku-Njane, WN and Makinde, OD, MHD nanofluid flow over a permeable vertical plate with convective heating, Journal of Computational and Theoretical Nanoscience, 11(3), 667–675, 2014.

[10] Nagler, J, Jeffery-Hamel flow of non-Newtonian fluid with nonlinear viscosity and wall friction, Applied Mathematics and Mechanics, 38(6), 815–830, 2017.

[11] Boyd, John P, Chebyshev and Fourier spectral methods, Courier Corporation, 2001.